Diffusion rates of Cu adatoms on Cu(111) in the presence of an adisland nucleated at fcc or hcp sites

Mihai-Cosmin Marinica,[1] Cyrille Barreteau,[1] Daniel Spanjaard,[2] and Marie-Catherine Desjonquères[1]

[1]*CEA Saclay, DSM/DRECAM/SPCSI, Bâtiment 462, F-91191 Gif-sur-Yvette, France*

[2]*Laboratoire de Physique des Solides, Université Paris Sud, Bâtiment 510, F-91405 Orsay, France*

The surface diffusion of Cu adatoms in the presence of an adisland at fcc or hcp sites on Cu(111) is studied using the embedded atom model potential derived by Mishin *et al.* [Phys. Rev. B **63**, 224106 (2001)]. The diffusion rates along straight (with close-packed edges) steps with (100) and (111)-type microfacets (respectively, step *A* and step *B*) are first investigated using the transition state theory in the harmonic approximation. It is found that the classical limit beyond which the diffusion rates follow an Arrhenius law is reached above the Debye temperature. The Vineyard attempt frequencies and the (static) energy barriers are reported. Then a comparison is made with the results of more realistic classical molecular dynamic simulations which also exhibit an Arrhenius-type behavior. It is concluded that the corresponding energy barriers are completely consistent with the static ones within the statistical errors and that the diffusion barrier along step *B* is significantly larger than along step *A*. In contrast the prefactors are very different from the Vineyard frequencies. They increase with the static energy barrier in agreement with the Meyer-Neldel compensation rule and this increase is well approximated by the law proposed by Boisvert *et al.* [Phys. Rev. Lett. **75**, 469 (1995)]. As a consequence, the remaining part of this work is devoted to the determination of static energy barriers for a large number of diffusion events that can occur in the presence of an adisland. In particular, it is found that the corner crossing diffusion process for triangular adislands is markedly different for the two types of borders (*A* or *B*). From this set of results the diffusion rates of the most important atomic displacements can be predicted and used as input in kinetic Monte Carlo simulations.

I. INTRODUCTION

The diffusion of adatoms on metal surfaces is still the subject of very active research.[1,2] Indeed, it plays a crucial role in crystal growth which is important to master in view of the applications, for instance in nanotechnologies. The more the growth is understood at an atomic level, the more the fabrication processes can be controlled in order to obtain a better quality of the device performances.

As a starting point, homoepitaxial systems can be used as models since effects such as interdiffusion processes are excluded and, even though lattice mismatch exists in atomic scale homoepitaxial nanostructures,[3] it is usually not so important as in heteroepitaxial systems. A large number of theoretical and experimental works has been devoted to homoepitaxial growth, e.g., on Pt,[4–8] Cu,[9–11] Ag,[12,13] Rh,[14–16] Al.[17–19] In this respect, the understanding of adisland shapes is of fundamental importance since they can indirectly influence the growth mode. The (111) surface of fcc metals is particularly interesting due to the observation of fractal as well as two- (2D) or three- (3D) dimensional compact adislands depending on the temperature.[6,7,20] Actually, the adisland morphology and its evolution with temperature result from a competition between thermodynamics and kinetic phenomena depending on the activation (or not) of various diffusion processes. The shape of adislands is governed by thermodynamics when the temperature is such that the adisland is able to relax to its equilibrium configuration during the time interval separating the incorporation of two consecutive atoms. In this case the shape of adislands on a (111)

fcc surface is determined by the ratio of two step energies since two types of steps with close-packed edges exist on this surface, the *A* step with a ledge of (100)-type orientation and *B* step with a ledge of (111)-type. The anisotropy ratio of the two step energies $E_{\text{step}}^A/E_{\text{step}}^B$ is most often very close to unity [for instance, using the Mishin *et al.*[21] potential for Cu, we have found $E_{\text{step}}^A=263$ meV and $E_{\text{step}}^B=265$ meV (Ref. 22)] and therefore the adisland shape derived from the Wulff theorem is an almost regular hexagon exhibiting threefold symmetry with edges corresponding to the smallest step energy slightly longer than the other ones.[23] When kinetic effects dominate, the adisland morphology depends on the flux of atoms impinging on the surface as well as on the rates of adatom diffusion on terraces, along steps, around adisland corners and of adatom attachment to (detachment from) the adisland.

The most efficient tool to simulate the evolution of the adisland morphology is the kinetic Monte Carlo [KMC (Refs. 24–26)] method which needs as input the various rates of all the elementary atomic processes. Two types of processes are essential in this respect, the diffusion along steps (and its anisotropy between step *A* and step *B*), and the corner crossings to go from one edge to another. At low temperature when none of these processes are activated one expects a fractal growth if the impinging flux is not too small since diffusion is rapid on a flat (111) fcc surface (e.g., the activation energy is only 40 meV for Cu). When these two processes occur, compact adislands can grow. An intermediate situation is also possible corresponding to an activation of step diffusion while corner crossing is still frozen. How-

ever other physical properties may have some importance, for instance, the step on which adatoms or dimers preferentially bind and the kink dissociation process play a role on the adisland shape which can vary with temperature from triangles limited by *A* steps, to triangles limited by *B* steps with intermediate hexagonlike patterns.[4,6] The various possible sequences are extremely dependent on the details of the energy profile and the modification of a single barrier can lead to very different adisland shapes. Moreover the diffusion across a step plays a crucial role in the crystal growth mode (Volmer-Weber, Stransky-Krastanov or Frank Van der Merwe). Indeed during growth adatoms can be deposited either on a wide terrace or on a preformed adisland. In the former case, the atom will diffuse until it sticks to the adisland, whereas in the latter case the adatom needs very often to overcome an extra activation energy (Schwoebel barrier) to incorporate to the descending step edge. Depending on temperature a 3D growth can thus be initiated. Therefore we have carried out a very detailed analysis of the various possible diffusion processes of a copper adatom in the vicinity of an adisland. Two types of epitaxy will be considered in which adatoms occupy either normal fcc sites or faulted hcp sites. Actually the stacking fault energy is very small in copper and adisland nucleation has been observed at fcc sites on the nominally flat surface and at hcp sites on the Cu(21,21,23) vicinal surface.[11]

Many experiments based on field ion[27,28] and scanning tunnelling[2,29,30] microscopies have been devoted to the determination of surface diffusion coefficients. However their interpretation may be somewhat tricky since, apart from peculiar cases, several elementary processes are involved. On the theoretical side, diffusion rates have been deduced either from transition state theory (TST) in the harmonic approximation[22,31–33] (TST-HA), or using classical thermodynamical integration[34] (TI) (see the Appendix) or else from classical molecular dynamic (MD) simulations.[35–39] In the classical limit all theoretical approaches conclude that an Arrhenius law, $\Gamma = \Gamma_0 \exp(-\Delta E / k_B T)$, fits accurately the evolution of the diffusion rates with temperature in good agreement with experiments. On the basis of MD simulations it has been suggested that the barrier ΔE for diffusion along steps on Ag(111) and Au(111) might be different from the static barrier[35] whereas Boisvert *et al.*[34] found that the value of the static barrier for Cu on Cu(100) lies inside the error bars of the results obtained both with MD and TI methods. Actually a very good accuracy on ΔE (better than a few 10^{-2} eV) would need huge simulation times. Furthermore the Arrhenius law being obviously approximate, the separation between a prefactor and an exponential term is somewhat arbitrary as will be discussed in Sec. II B. Finally it must be emphasized that in KMC simulations the prefactor is most often taken as independent of the barrier height. However, this assumption has already been questioned in the literature.[18,36,40–42] Indeed, it has been observed that an increase of this barrier is somewhat compensated by an increase of the prefactor. This effect is known as the Meyer-Neldel compensation rule[43] and may have important consequences by allowing an inversion of the diffusion rates corresponding to the most important processes at a given temperature. This point will be discussed in Sec. III C.

From the above remarks, it is clear that any investigation of diffusion processes should begin with the determination of the (static) potential energy barriers. A limited number of barriers concerning high symmetry systems have been calculated using *ab initio* codes[44] but these codes are too computer time demanding when the symmetry is low, i.e., when the number of elementary diffusion processes is large. One must then rely on semiempirical potentials such as those derived from effective medium theory (EMT),[45] embedded atom model (EAM),[46,47] or second moment approximation (SMA).[48] Even with these simple models, unknown barriers are sometimes deduced using some approximations.[10] Even though these approximations are reasonable some effects can be missed as we will see in the following.

The aim of this work is the determination of the diffusion rates corresponding to most of the elementary diffusion processes that may occur during the growth of a single 2D adisland on Cu(111). After having briefly presented the potential used (Sec. II A) we study the diffusion of an adatom along step *A* and step *B* (Sec. III) using the two methods described in Sec. II B, namely the TST-HA approach (in the classical limit) and MD simulations. We show that the static activation barrier accounts quite well for the results of MD simulations. However, the prefactors obtained in the latter method are different from those given by TST-HA. Furthermore they are quite consistent with the Meyer-Neldel law proposed by Boisvert *et al.*.[36] As a consequence, in the remaining part of the paper, we limit ourselves to the determination of the static barriers for other diffusion events in the presence of straight steps (Sec. IV) or in the vicinity of steps with defects, for instance around corners and kinks (Sec. V). Conclusions are drawn in Sec. VI. Finally the Appendix briefly summarizes the TST-HA theory and the TI method.

II. FORMALISM

A. The potential

We have used in this work the EAM potential derived by Mishin *et al.*[21] for copper. In this model the total energy of an assembly of *N* atoms with respect to that of *N* isolated atoms is written as a function of all interatomic distances r_{ij},

$$E = \frac{1}{2} \sum_{i,j=1}^{N} V(r_{ij}) + \sum_{i=1}^{N} F(\rho_i), \qquad (1)$$

where ρ_i can be interpreted as a function proportional to the electron density induced at site *i* by the neighbors, i.e.,

$$\rho_i = \sum_{j \neq i} \rho(r_{ij}). \qquad (2)$$

The proportionality factor is chosen such that $\rho_i = 1$ for a bulk atom at equilibrium. The chosen reference energy implies that $V(r)$ and $\rho(r)$ vanish when *r* tends to infinity and $F(0) = 0$. The functions $V(r)$, $\rho(r)$, and $F(\rho)$ are fitted parametrized functions which, on the whole, contain 26 parameters. The 26 parameters are required to give exactly the bulk equilibrium lattice parameter, cohesive energy and bulk modulus and to fit selected properties of copper taken from

experiments or obtained by *ab initio* calculations. These properties are mainly related to the bulk phase and include in particular the stacking fault energy which is of a peculiar importance in the present work. More details can be found in Ref. 21. In addition, Mishin *et al.* have shown that their potential was able to reproduce many physical quantities not included in the fitting data base and, in particular, the surface energies of low index surfaces. Moreover we have already used this potential in a previous work.[22] First we verified that it gives other surface properties, like the step and kink energies, with numerical values very close to experimental data. Then we used it to study the diffusion of monomers, dimers and trimers on Cu(111) and our results were in very good agreement with STM observations. We are thus very confident in using this potential for the present problem.

B. Determination of diffusion coefficients along straight steps

The diffusion coefficients along straight steps (i.e., with a close-packed edge) have been calculated using two techniques. On the one hand, they can be derived from the TST (Ref. 49) by combining the determination of the minimum energy path and the calculation of the vibrational free energy in the framework of the HA and, on the other hand, using MD simulations. Indeed, as will be seen in the following, the most frequent diffusion event for an adatom attached to a straight step corresponds to jumps along this step since the barriers corresponding to other events are much higher. Thus this diffusion is essentially a one-dimensional problem.

1. Diffusion coefficients of an adatom along straight steps from TST-HA

From TST the surface diffusion coefficient $D(T)$ along straight steps at temperature T is related to the diffusion frequency (or diffusion rate) $\Gamma_{TST}(T)$ by

$$D(T) = \frac{1}{2}a^2\Gamma_{TST}(T) \qquad (3)$$

when the diffusion is assumed to proceed by uncorrelated jumps of length a between neighboring adsorption sites along the step (note that a increases slowly with T when thermal expansion is taken into account but in practice this effect is quite negligible). The diffusion frequency $\Gamma_{TST}(T)$ is given by

$$\Gamma_{TST}(T) = 2\frac{k_B T}{h}\exp(-\Delta F/k_B T), \qquad (4)$$

where ΔF is the difference of total free energy between the saddle point and the starting adsorption configuration (stable or metastable equilibrium). The factor 2 arises from the number ($n_c = 2$) of diffusion channels, i.e., $\Gamma_{TST}(T)$ is the diffusion frequency in *both* directions along the step. ΔF can be split into two contributions,

$$\Delta F = \Delta E + \Delta F_{vib} \qquad (5)$$

ΔE is the potential energy barrier, i.e., the difference in total energy [Eq. (1)] between the saddle point and the equilibrium configuration. This static diffusion barrier ΔE can be

calculated by determining the minimum energy path using the Ulitsky-Elber algorithm[50] which we already used with success in our study of the surface diffusion on the flat Cu(111) surface.[22] For technical details the reader is referred to this latter reference. The quantity $\Delta F_{vib} = \Delta U_{vib} - T\Delta S_{vib}$ is the contribution of vibrations to the variation of the free energy (with obvious notations). In the HA (see the Appendix), ΔF_{vib} is given by

$$\Delta F_{vib} = k_B T \int_0^{\nu_{max}} \ln\left[2\sinh\left(\frac{h\nu}{2k_B T}\right)\right]\Delta n(\nu)d\nu, \qquad (6)$$

where $\Delta n(\nu)$ is the difference between the vibrational densities at the saddle point and at equilibrium which are computed from the eigenvalues of the dynamical matrix. Note that at the saddle point one of the eigenvalues ν_p^2 is negative. This eigenvalue is excluded from the vibration density and, consequently,

$$\int_0^{\nu_{max}} \Delta n(\nu)d\nu = -1. \qquad (7)$$

Thus in this TST-HA model, the diffusion rate is

$$\Gamma_{TST}^{HA}(T) = 4\frac{k_B T}{h}\frac{\displaystyle\prod_{p=1}^{3N}\sinh\left(\frac{h\nu_p^e}{2k_B T}\right)}{\displaystyle\prod_{p=1}^{3N-1}\sinh\left(\frac{h\nu_p^s}{2k_B T}\right)}\exp(-\Delta E/k_B T)$$

$$= \Gamma_0^{HA}(T)\exp(-\Delta E/k_B T) \qquad (8)$$

if we call ν_p^e and ν_p^s the (real) eigenfrequencies for the equilibrium and saddle point configurations and $N+1$ the total number of atoms, i.e., including the adatom. Note that the three free translational modes (of zero frequency) have been excluded from the spectra. It is seen that the prefactor $\Gamma_0^{HA}(T)$ depends in general on T and, consequently, $\Gamma_{TST}^{HA}(T)$ does not follow an Arrhenius law.

Let us examine the limits of low and high temperatures. In the low temperature limit $\Delta S_{vib} \to 0$ and $\Delta U_{vib}(T) = \Delta U_{vib}(0) + \mathcal{O}(T^4)$ (Ref. 51) so that

$$\Gamma_{TST}^{HA}(T) \simeq 2\frac{k_B T}{h}\exp\{-[\Delta E + \Delta U_{vib}(0)]/k_B T\}. \qquad (9)$$

In the high temperature limit we get

$$\Gamma_{TST}^{HA}(T) = 2\nu_0\exp(-\Delta E/k_B T) \qquad (10)$$

in which ν_0 is the Vineyard attempt frequency given by[52]

$$\nu_0 = \frac{\displaystyle\prod_{p=1}^{3N}\nu_p^e}{\displaystyle\prod_{p=1}^{3N-1}\nu_p^s}. \qquad (11)$$

Thus, in this limit, $\Gamma_{TST}^{HA}(T)$ follows an Arrhenius law with a diffusion barrier ΔE and a prefactor $2\nu_0$.

In this TST-HA approach the deviation from the Arrhenius law comes from quantum effects. We will see in the follow-

ing that these effects become negligible above the Debye temperature [T_D=343 K for Cu (Ref. 53)]. Accordingly the classical molecular dynamics approach, which we will briefly describe in the next section, is fully justified above T_D.

2. Diffusion coefficients along straight steps from MD simulations

The motion of the $N+1$ atoms is studied by MD simulations in which the Newton equations of motion in the potential given by Eq. (1) is solved using the Verlet algorithm in its velocity form. The simulation is carried out in the temperature range 350 K–600 K and no correction of the temperature is needed since quantum effects can be neglected.[54] The thermal expansion of the Cu crystal is derived from MD simulations in the bulk and the nearest neighbor distance is fitted by a=2.553+2.516 $10^{-5}T$+1.194 $10^{-8}T^2$ in Å. After an equilibration period, the motion of the adatom is observed during another period t_{run} and the trajectory of the adatom is recorded. This trajectory is analyzed by assuming that the diffusion proceeds by uncorrelated and discrete jumps. At this point, we must emphasize the differences between MD and TST. The basic assumption in TST is that each crossing of a dividing surface containing the saddle point corresponds to a diffusion event and thus "recrossing effects" are ignored.[49] This is not the case in MD since recrossing events can be identified, i.e., they occur when the adatom turns back in a very short time after having crossed the dividing surface. Moreover in Eq. (3) each diffusion event is assumed to be a jump of length a while long jumps of length na can occur in MD. Finally, anharmonic effects are included since the forces are calculated from the exact expression of the potential.

The diffusion coefficient is given by the Einstein formula,

$$D(T) = \lim_{t \to \infty} \frac{\langle [\mathbf{r}(t)]^2 \rangle}{2t}, \qquad (12)$$

where

$$\mathbf{r}(t) = \sum_{i=1}^{N_S} n_i \mathbf{r}_i, \qquad (13)$$

N_S is the total number of jumps during the time interval t, $n_i\mathbf{r}_i$ is the displacement vector corresponding to the ith jump (n_i=1,2,3,... for a simple, double, triple, etc., jump, respectively, and r_i=a) and, for uncorrelated jumps (i.e., $\langle \mathbf{r}_i \cdot \mathbf{r}_j \rangle$=0), if t_{run} is large enough,

$$D(T) = \frac{a^2}{2} \sum_{i=1}^{N_S} \frac{n_i^2}{t_{run}} = \frac{a^2}{2} \sum_n \frac{N_n}{t_{run}} n^2 = \frac{a^2}{2} \Gamma^{MD}(T), \qquad (14)$$

where N_n is the number of jumps of length na observed during the period t_{run}.

The discrimination between the accepted and rejected diffusion events and between the different jump lengths is done with the same criterion as in the work of Ferrando and Tréglia.[35] Let us call τ_{th} the thermal time given by
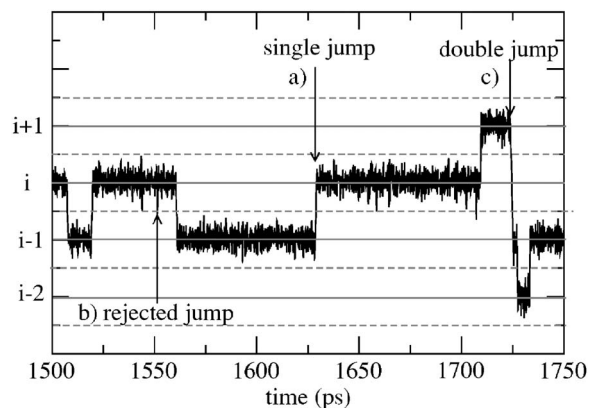

FIG. 1. Typical time evolution of the position of an adatom along a step. The adatom starts from site i and the unit along the ordinate axis is the nearest neighbor spacing a. The adatom is considered to be at site i if its coordinate lies in the interval [$i-1/2,i+1/2$]. The rejected, single and double jumps are marked by arrows.

$$\tau_{th} = a \left(\frac{m}{k_B T} \right)^{1/2}, \qquad (15)$$

where m is the mass of the adatom, i.e., τ_{th} is simply the time to go over the lattice spacing for a particle with an energy $k_B T$, for example, τ_{th}=1 ps at T=500 K. The diffusing atom is considered to have resided at a given site if the time spent on this site is longer than τ_{th}. This is illustrated in Fig. 1. For instance the case (a) corresponds to a single jump since the time spent at sites $i-1$ and i is longer than τ_{th}, whereas no jump is recorded in the case (b) since the time spent at $i+1$ is too short (recrossing event). Finally the case (c) corresponds to a double jump since the time spent at site i is too short.

The usual method to analyze the temperature dependence of Γ^{MD} is to draw an Arrhenius plot, i.e., $\ln \Gamma^{MD}(T)$ vs $1/k_B T$.[34–39] Most often a quasilinear behavior is observed, the larger the number of recorded diffusion events (i.e., the smaller the statistical error), the smaller the deviation from linearity. As a consequence, $\Gamma^{MD}(T)$ can be approached by an Arrhenius law,

$$\Gamma^{MD}(T) = \Gamma_0^{MD} \exp(-\Delta E^{MD}/k_B T) \qquad (16)$$

in which the parameters Γ_0^{MD} and ΔE^{MD} are obtained by a least mean square fit.

It is then found that ΔE^{MD} differs slightly from the static barrier ΔE. This small discrepancy may be due to statistical errors. Actually, as we will illustrate in the following (see Fig. 5), if the fit is carried out by setting ΔE^{MD}=ΔE the corresponding straight line is also contained inside the error bars. Furthermore, if real physical effects were responsible for the variation between ΔE^{MD} and ΔE, then ($\Delta E^{MD}-\Delta E$) should be a function of temperature. Consequently the Arrhenius law is not strictly obeyed and the splitting of Γ^{MD} into a prefactor and an exponential is somewhat arbitrary. However if the variation of ($\Delta E^{MD}-\Delta E$) is of the first order in T, then the Arrhenius law remains almost strictly obeyed with a slope equal to ΔE.
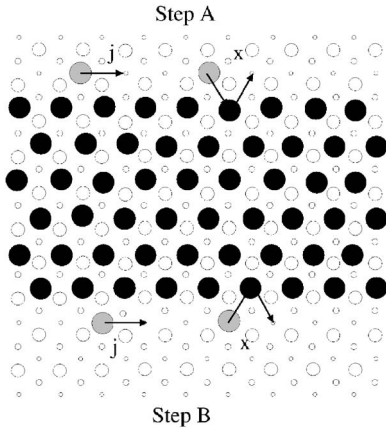
FIG. 2. Diffusion processes of a Cu adatom (gray circles) along the steps A and B limiting a stripe in fcc geometry on Cu(111), j (jump) and x (exchange) mechanisms. The filled black circles are the atoms of the stripe and the atoms of the substrate are denoted as open circles with a size decreasing when going towards the inside of the substrate.

Actually, using TI (see the Appendix) Boisvert et al.[34] have shown that the diffusion frequency can be written as an Arrhenius-type law in which the prefactor Γ_0^{TI} and the barrier ΔE^{TI} are almost independent of temperature in the range 100–800 K for surface diffusion of Cu on Cu(100). Moreover, by comparing the TI method with MD simulations, these authors observed that the static barrier ΔE lies always inside the error bars of ΔE^{TI} and ΔE^{MD}. We will see in the following that, similarly, our results on the diffusion of Cu along straight steps of Cu(111) can be fitted nicely by assuming $\Delta E^{MD} = \Delta E$.

III. DIFFUSION OF A Cu ADATOM ALONG STRAIGHT STEPS ON Cu(111)

A. The geometry

It is well known that there are two types of steps with close-packed edges on Cu(111), the step A with a (100) ledge and the step B presenting a $(\bar{1}11)$ ledge. The study of the surface diffusion along or across these steps is a prerequisite to investigate the growth of large Cu adislands on Cu(111). These adislands are expected to be bordered by steps of type A or B and, out of equilibrium, may be or not in stacking fault[11] since the stacking fault energy is rather small in copper. In the first case the atoms occupy hcp sites while, in the second, they are located at fcc sites. Thus we have to study four geometries, step A or step B for adislands at fcc or hcp sites.

In practice a supercell containing $p_1 \times p_2$ two-dimensional unit cells with N_p layers is built to represent the Cu(111) surface. On this supercell a stripe of N_{stripe} close-packed atomic rows is added at fcc or hcp sites. This stripe is thus limited by an A step on one side and a B step on the other one (Fig. 2). The number N_{stripe} of rows is large enough to avoid any interaction between the two steps. On each side of this stripe (A and B edges) an adatom is deposited. Finally, the usual periodic boundary conditions are applied.

TABLE I. Diffusion barriers ΔE_j^{rel} and corresponding prefactors Γ_0^{HA} (ν_0 is the Vineyard attempt frequency) for Cu self-diffusion (jump mechanism) along A and B steps on the (111) surface, in regular fcc and faulted hcp geometries. In the last line we give the diffusion barriers ΔE_e for the exchange mechanism shown in Fig. 2. For comparison, we also report in the first line the values of the barriers ΔE_j^{unrel} calculated for an unrelaxed substrate.

Step type	A		B	
Stripe geometry	fcc	hcp	fcc	hcp
ΔE_j^{unrel} (meV)	326	315	536	529
ΔE_j^{rel} (meV)	247	235	312	302
$\Gamma_0^{HA} = 2\nu_0$ (THz)	7.84	8.54	7.44	8.04
ΔE_e (meV)	1532	1512	1715	1691

B. Diffusion of adatoms in the TST-HA approach

We have first carried out static calculations from which the minimum energy path between two first neighbor adsorption sites along A and B steps is determined for the jump and exchange diffusion mechanisms shown in Fig. 2. These calculations were performed on a large supercell, the slab representing the surface contained (11×11) 2D unit cells and was 10 layer thick. The stripe was made of four atomic rows. In view of the large number of atoms in this supercell, only the point $\mathbf{k}_\parallel = 0$ in the surface Brillouin zone was used to calculate the phonon frequencies. Similarly to our previous work,[22] the equilibrium structure was deduced from the conjugate gradient method and convergence was achieved when all the forces were smaller than 10^{-3} eV/Å. The minimum energy path was determined using the Ulitsky-Elber algorithm[50] and the iteration process was stopped when all the forces perpendicular to the path were less than 3×10^{-2} eV/Å.

The results show that the adsorption energy of an adatom along a B step is favored by 7 meV with respect to an A step. This difference in energy is probably too small to have any influence on the island growth morphology and could not be at the origin of an asymmetry between A and B steps. In contrast the diffusion paths along step A and step B for the jump mechanism are quite different. While along step A the diffusion proceeds by fcc→hcp (saddle point)→fcc jumps on the (111) terrace, along step B the path can be approximated by a displacement along the channel of a (011) microfacet which can be considered as the ledge. Indeed let us recall that the (111)fcc surface with periodic monoatomic B steps can be denoted either as $(p+1)(111) \times (\bar{1}11)$ or as $p(111) \times (011)$.[55] However it is difficult to find qualitative arguments to determine the step on which the diffusion is faster. Indeed, the diffusion along these two steps has been studied for other elements in the literature[35] and it was found that, while Ag behaves as Cu in this respect, the diffusion barrier is lower along step B in Au. In order to elucidate the role played by atomic relaxation, we have carried out the same calculations but in which the substrate was considered as a perfect termination of the bulk crystal. The corresponding results (ΔE_j^{unrel}) are given in Table I. These results can be

understood qualitatively by simple bond breaking arguments. Indeed when going from the equilibrium site roughly one nearest neighbor bond is broken when the adatom diffuses along step *A* whereas one nearest neighbor bond is broken and two other bonds are significantly expanded at the saddle point of step *B*. Consequently the barrier is much higher along step *B* than along step *A*. However, it is seen that the lowering of the barriers due to relaxation is important. Moreover the difference in the diffusion barriers along the two type of steps is strongly decreased. It is interesting to note that, when comparing with the results of Ref. 35, this difference decreases when going from Cu to Ag and changes sign for Au. This variation of behavior may be due to increasing relaxation effect. Indeed, when using a second moment potential, the importance of surface relaxation increases when p-$2q$ increases, p and q being the parameters governing the exponential decrease of the repulsive and attractive term, respectively.[56] The values of p-$2q$ are 4.96 (Cu), 3.38 (Ag), and 1.90 (Au).[57] Thus relaxation effects are expected to increase when going from Cu to Ag and Au and could be strong enough in Au to make the diffusion easiest along step *B*, contrary to Cu. Finally we have found that the strain field does not affect the energy balance between hcp and fcc sites in Cu.

The resulting energy barriers presented in Table I show that diffusion always proceeds by the jump mechanism (the energy barrier for the exchange mechanism being extremely high) and is expected to be faster along step *A* than along step *B* since its energy barrier is smaller by about 60 meV. Moreover, for both steps the diffusion barrier along a hcp stripe is slightly smaller by 10 meV than along a fcc stripe, i.e., the variation of the energy barrier between *A* and *B* steps is almost exactly the same in fcc and hcp geometries, 65 meV and 67 meV, respectively. Consequently from static calculations, the asymmetry between the diffusion along *A* and *B* steps should be rather similar in fcc and hcp geometries. Then we have calculated the phonon spectrum for adatoms at the equilibrium and saddle point configurations, from which the prefactor $\Gamma_0^{HA}(T)$ is deduced. In Fig. 3(a) we show the evolution with temperature of this prefactor, it is seen that the high temperature limit is attained above $\simeq 300$ K, i.e., close to the Debye temperature of Cu. This limit is equal to twice the Vineyard attempt frequency [Eq. (11)] and is given in Table I. Accordingly, above 300 K, the diffusion rate follows an almost perfect Arrhenius law which is actually almost undistinguishable from its asymptotic limit $2\nu_0 \exp(-\Delta E/k_B T)$ [Fig. 3(b)]. One notes that the prefactors are not very dependent on the geometry and thus, in this model, the diffusion rate is governed almost entirely by the exponential term. The diffusion along step *A* is indeed faster than along step *B* and the motion is slightly easier in the hcp geometry. In order to quantify the asymmetry between step *A* and step *B* we have also calculated the ratio Γ_A/Γ_B of the diffusion rates along the two types of steps (see Fig. 4). This ratio is very similar in hcp and fcc geometries, it increases as the temperature decreases and typically adatom diffusion processes are approximately 4 and 6 times faster along step *A* than along step *B* at 600 K and 450 K, respectively.
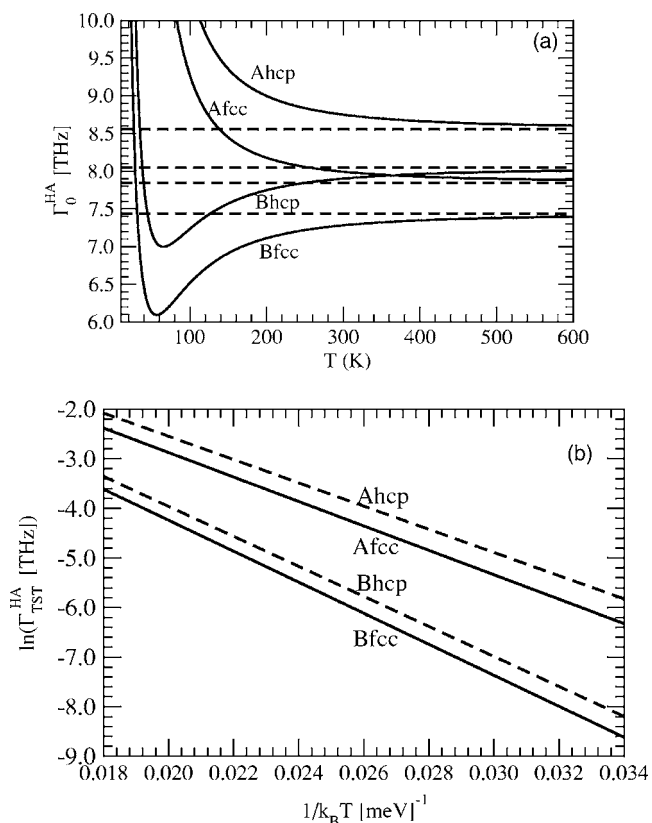

FIG. 3. (a) Prefactors $\Gamma_0^{HA}(T)$ of the jump rate, obtained from the TST-HA model, for Cu diffusion along *A* and *B* steps on Cu(111), in fcc and hcp geometries. (b) Arrhenius plots of $\Gamma_{TST}^{HA}(T)$ corresponding to the four geometries in the temperature range 340 K–645 K.

C. Diffusion of adatoms from MD simulations

The simulations have been performed on a (11×11) slab containing 16 layers with a stripe made of four atomic rows in fcc sites on one side of the slab and in hcp sites on the other side. One adatom is deposited along each of the four close-packed step edges of the two opposite stripes. This procedure allows to obtain with a single simulation box, the
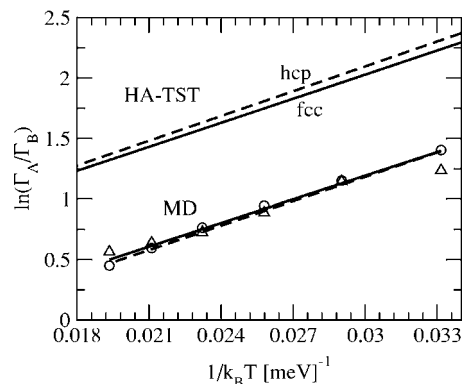

FIG. 4. Arrhenius plots of the ratio Γ_A/Γ_B of the jump diffusion rates for a Cu adatom along *A* and *B* steps on Cu(111) in fcc and hcp geometries as deduced from the TST-HA model and MD simulations (open circles, fcc geometry; open triangles, hcp geometry).

TABLE II. Statistics of single (N_1), double (N_2), triple (N_3), and rejected single (N_r) jumps for the diffusion of a Cu adatom along step A and step B on Cu(111), in fcc and hcp geometries, from MD simulations. The total simulation time t is given for each temperature T.

Step type																	
		A								*B*							
Stripe geometry		fcc				hcp				fcc				hcp			
T(K)	t(ns)	N_1	N_2	N_3	N_r	N_1	N_2	N_3	N_r	N_1	N_2	N_3	N_r	N_1	N_2	N_3	N_r
350	165.9	277	3	0	258	401	9	0	180	71	0	0	137	115	3	0	82
400	98.0	391	17	1	382	608	19	1	343	127	3	1	259	193	7	0	187
450	77.7	696	21	1	582	953	30	2	553	275	8	0	478	377	16	1	384
500	58.8	960	33	3	875	1294	38	3	727	447	19	0	779	544	31	5	561
550	39.2	977	55	4	993	1323	60	3	815	540	26	4	842	603	50	4	722
600	30.8	1159	57	7	1020	1448	88	9	926	709	38	7	1249	769	57	8	910

four trajectories from which the diffusion coefficients are extracted. We have performed a series of MD simulations for temperatures ranging from 350 K to 600 K. The classical equations of motion were integrated with a time step of 3.5 fs. The system was first equilibrated for about 12 ps. We have verified that with a time step of 3.5 fs the system is well behaved since the drift in the total energy of the system is less than 10^{-4}% and the ratio of the root mean square fluctuations $\sigma(E)$ of the total and kinetic energies $\sigma(E_T)/\sigma(E_K)$ is always less than 2%. In the considered temperature range the far most frequent event is a jump along the step, however from time to time an extra event occurs, such as the formation of a dimer with an atom escaping from the step (see Sec. V B). To avoid the occurrence of such "unwanted events," we have preferred to perform a number of independent simulations rather than a single and longer one. At each temperature the total simulation time was chosen in order to get a meaningful statistics, i.e., it decreases when the temperature increases. The diffusion coefficient can be calculated either from the Einstein relation [Eq. (12)], or from Eq. (14) which assumes uncorrelated discrete jumps. We have found that the two methods give practically the same results showing that the jumps are indeed uncorrelated. In the following the results will be analyzed using the second approach which has the advantage of allowing an estimation of statistical errors. Thus the analysis of the trajectory consists in an enumeration of the various jumps (accepted or rejected) occurring during the simulation time. The statistics of the number of jumps is presented in Table II. It is seen at first glance that significant differences with TST-HA are expected since the transmission coefficient κ [i.e., the fraction $N_1/(N_1+N_r)$ of accepted jumps] is far from being unity.

In Fig. 5 we show the Arrhenius plots of $\Gamma^{MD}(T)$ for the four geometries with error bars corresponding to the standard deviation. We have first carried out a least mean square fit with the two parameters Γ_0^{MD} and ΔE^{MD}. Similarly to the results of Boisvert *et al.*[34] on the surface diffusion of Cu on Cu(100), we find that ΔE^{MD} is quite close to the static barrier ΔE (see Table III) and the fitted straight line lies inside the error bars demonstrating the quality of the statistics. However, as already discussed in Sec. II B 2 it is advisable to compare with a fit in which the barrier has been fixed to its static value. The corresponding fits shown in Fig. 5 are

nearly as good as the previous ones. Moreover the associated prefactors become quite comparable in fcc and hcp geometries in contrast with the previous fits for which the prefactor for the B step in the hcp geometry was much smaller than in the fcc geometry. This does not seem physically reasonable but is most probably due to the uncertainty on ΔE^{MD} since a small error in ΔE^{MD} must be compensated by a large variation of the prefactor in order to give the same value of Γ^{MD}. Thus we have adopted the values of the prefactors Γ_0^{MD} derived from the fit in which $\Delta E^{MD}=\Delta E$. In this case it is seen from Tables I and III that Γ_A/Γ_B as deduced from MD is about twice smaller than the corresponding value in TST-HA (see Fig. 4). Indeed in the TST-HA model the prefactors are very similar for steps A and B while, from MD simulations, the prefactor corresponding to steps B, which have the highest diffusion barrier, is about twice that of step A. We will
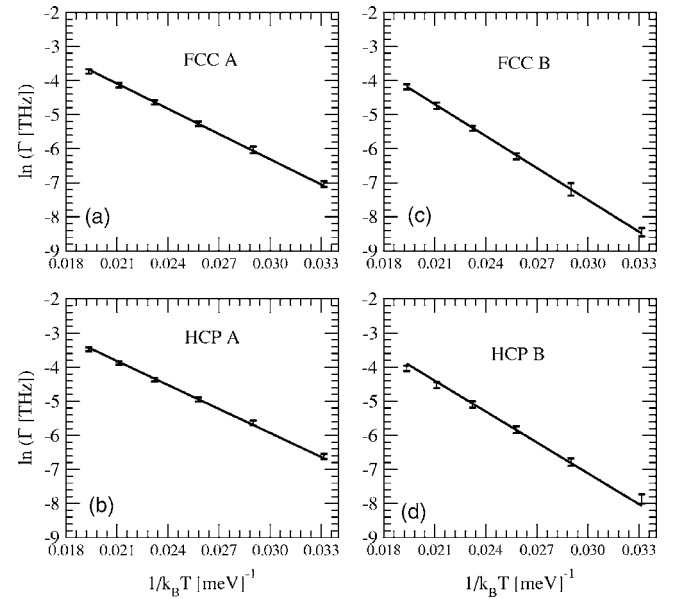

FIG. 5. Arrhenius plots of the MD jump rates for Cu diffusion along straight steps on Cu(111) in fcc and hcp geometries. The error bars give the statistical error. The straight line is a least mean square fit in which the energy barrier has been fixed to its static value. (a) Step A in fcc geometry; (b) step A in hcp geometry; (c) step B in fcc geometry; (d) step B in hcp geometry.

TABLE III. Transmission coefficients $\langle\kappa\rangle$ averaged over temperature, energy barriers, and prefactors derived from MD simulations, (a) both parameters ΔE^{MD} and Γ_0^{MD} have been obtained from a least mean square fit; (b) Γ_0^{MD} has been obtained from a least mean square fit with ΔE^{MD} fixed at its static value ΔE.

	Step type	A		B	
	Stripe geometry	fcc	hcp	fcc	hcp
	$\langle\kappa\rangle$	0.52	0.64	0.36	0.50
(a)	ΔE^{MD} (meV) fitted	239	226	308	279
	Γ_0^{MD} (THz) fitted	5.0	4.9	11.6	7.8
(b)	ΔE (meV) fixed	247	235	312	302
	Γ_0^{MD} (THz) fitted	6.0	6.1	12.8	14.0

now give a physical interpretation for this difference.

It is frequently found that when the activation energy increases within a family of processes, the prefactor also increases. Thus, in the expression of the process rate, the increase of the prefactor somewhat "compensates" for the decrease in the Arrhenius exponential term governing the dependence on temperature. This effect is known as the Meyer-Neldel compensation law.[43] It has been investigated by Boisvert *et al.*[36] in the particular case of surface self-diffusion by means of MD simulations. By studying jump and exchange processes on the (100) and (111) surfaces of elements belonging to the end of the transition series or to noble metals, they have proposed the following law for the prefactors:

$$\Gamma_0 = \Gamma_{00} \exp(\Delta E/\Delta_0)^{\alpha}. \qquad (17)$$

From theoretical models[58,59] the exponent α is expected to lie in the range 0.5–1 depending on the nature of the excitations that give rise to the activated process. For acoustical phonons, a simple phenomenological model predicts $\alpha = 3/4$ and a characteristic energy Δ_0 of the order of 2–3 times larger than a typical phonon energy (for instance $h\nu = k_B T_D$ where T_D is the Debye temperature). Actually Boisvert *et al.*[36] have found that their results can be reasonably fitted with $\alpha = 0.7$, $\Delta_0 = 74$ meV, and $\Gamma_{00} = 0.74$ THz.

As already stated, our MD data for steps A and B obey the same trend since Γ_0^{MD} increases with ΔE. Thus it is interesting to add the corresponding data (see Fig. 6) on the plot giving the logarithm of the prefactor versus $(\Delta E)^{0.7}$ which should be a straight line (Fig. 3 of Ref. 36). Our results are quite close to the straight line obtained by Boisvert *et al.*

Let us now comment on the differences between the TST-HA and MD approaches. As already mentioned, MD simulations take into account the transmission coefficient κ and anharmonic effects. From our simulations κ does not vary significantly with temperature. From Table III, it is seen that on average $\kappa_A/\kappa_B \simeq 1.5$ for both geometries. As a consequence the increase of the prefactor for step B with respect to step A is not due to the transmission coefficient but rather to anharmonic effects which, as discussed by Boisvert *et al.*,[34,36] lead to multiphononic excitations. The prefactor is
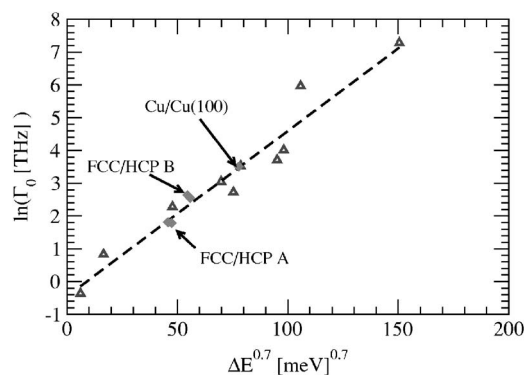

FIG. 6. Plot of $\ln\Gamma_0$ as a function of $\Delta E^{0.7}$. The points represented by empty triangles are taken from Boisvert *et al.* (Ref. 36) and refer to various surface self-diffusion processes on low index surfaces of Au, Ag, Ni, and Pd. The points indicated by arrows (filled black diamonds) are derived from our molecular dynamic simulations along A and B straight steps on Cu(111) in fcc and hcp geometries and diffusion of Cu on Cu(100). The dashed line is the fit corresponding to Eq. (17).

then proportional to the number of ways of assembling these excitations. This gives rise to an entropy factor increasing with the barrier height (see the Appendix). This interpretation is consistent with the absence of a Meyer-Neldel effect in the TST-HA model which has already been noted by other authors.[44]

Finally, in order to confirm the Meyer-Neldel rule, we have also carried out MD simulations for Cu adatoms on Cu(100) in the temperature range 500–750 K in which we have found that diffusion proceeds by simple hopping. Within statistical errors, the static barrier (502 meV) accounts well for the slope of the Arrhenius plot and the associated prefactor[60] ($\Gamma_0 = 33.4$ THz) obeys accurately the law proposed by Boisvert *et al.*[36] as seen in Fig. 6. As a conclusion, it is clear that the prefactor should increase with the (static) barrier height ΔE. Nevertheless, we must note that this variation of the prefactor is most often neglected in KMC simulations. This may have important effects since, with this assumption, the mechanism which has the lowest energy barrier occurs the most frequently at any temperature. On the contrary, if the prefactor increases with ΔE, a process with a higher ΔE may become the most frequent above a given temperature. For instance Boisvert and Lewis[38] have found an inversion of the dominant diffusion mechanism from simple hopping to exchange above $\simeq 750$ K for Cu on Cu(100) that we have also observed in our MD simulations with the Mishin potential. As shown by Ruggerone *et al.*[18] an inversion can change the island growth shapes of Al on Al(111) which can switch from triangles with A borders to triangles with B borders when the temperature increases. In the absence of systematic calculations of the prefactors, the law proposed by Boisvert *et al.* [Eq. (17)] can be used to get a reasonable estimate of this variation. Thus, in the remaining part of this work, we will limit ourselves to the determination of the static diffusion barriers.
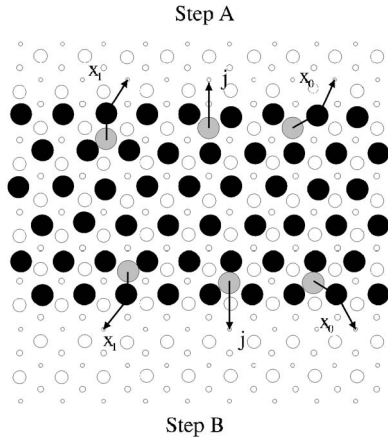
Step A

Step B

FIG. 7. Diffusion processes of a descending adatom across the A and B steps limiting a stripe in fcc geometry on Cu(111), by jump (j) or exchange (x_0 and x_1) mechanisms. The atoms are represented as in Fig. 2.

IV. OTHER DIFFUSION EVENTS IN THE PRESENCE OF STRAIGHT STEPS

A. Diffusion of adatoms across straight steps: Schwoebel barrier

When an adatom is deposited on an adisland it wanders on its surface until either it meets a group of adatoms already present on this adisland or it comes down the step edge by diffusing across the step. However the additional barrier (called the Schwoebel barrier) felt by the adatom for the latter process is often rather high relative to the barrier (41 meV from fcc to hcp sites, 36 meV from hcp to fcc sites[22]) encountered on the flat surface and the probability that an adatom crosses the step is small. As a consequence it is often assumed that the flux of adatoms towards the step comes from the lower terrace. The "traditional picture" of an adatom "jumping" down the step (process j of Fig. 7) and therefore losing one nearest neighbor in the diffusion process usually leads to high energy barriers but another type of diffusion process exists, i.e., the exchange mechanism in which the adatom takes the place of a step atom which becomes an adatom attached to the step (processes x_0 and x_1 of Fig. 7). In Table IV we present the energy barriers corresponding to the three types of diffusion mechanisms across the steps A and B on an adisland in fcc and hcp configurations. Interestingly the energy barriers for a jump mechanism are almost the same (around 510 meV) in all cases, but the exchange

TABLE V. Energy barriers for the formation and dissociation of a step dimer along A and B steps in fcc and hcp geometries.

Step	A		B	
Geometry	fcc	hcp	fcc	hcp
Dimer dissociation	520	509	568	560
Dimer formation	207	197	262	255

mechanism has a lower barrier by $\simeq 200$ meV for the process x_0 ($\simeq 130$ meV for x_1) on step A and $\simeq 400$ meV for both exchange processes on step B. A strong anisotropy is therefore found between step A and step B. The Schwoebel barrier is thus only $\simeq 50$ meV for step B while it is around 250 meV and 300 meV for x_0 and x_1, respectively, on step A. The existence of a low Schwoebel barrier across step B is in agreement with the previous EAM calculations by Trushin *et al.*.[47] This difference can be explained qualitatively by looking at Fig. 7. On step B, the step atom is pushed by the adatom towards the nearest fcc site in front of it (by passing over a bridge site), simultaneously the adatom takes its place while the step atom becomes a step adatom at an fcc site. During the motion towards the saddle point the involved bonds are only moderately compressed or expanded. This is not the case for the step A on which the displaced step atom cannot move perpendicularly to the step edge since it must go over an atop position which is clearly energetically unfavorable. The motion towards one of the two nearest hcp sites is also somewhat blocked since in this motion the bond of the displaced step atom with one of its two nearest neighbor step atoms is strongly shortened. The low Schwoebel barrier on step B could play a role in the fast decay of double layer Cu adislands on Cu(111) observed in experiments[61,62], even if the scenario of this phenomenon is more complicated.[63]

B. Formation and diffusion of dimers

A step adatom diffusing along the step will possibly meet another single adatom to form a step dimer, or stick to a kink. The latter case will be discussed later (see Sec. V). Let us first mention that the adsorption energy of a dimer along a B step is favored by 5 meV with respect to an A step. In Table V we present the energy barriers for the formation and dissociation of a dimer (see Fig. 8). As expected the diffusion of an adatom is favored by the proximity of another adatom,

TABLE IV. Diffusion barriers of an adatom descending or ascending a step (A or B) by various mechanisms, jump (j), exchange (x_0 or x_1) (see Fig. 7) for fcc and hcp geometries. The directions ▶ and ◀ correspond to descending and ascending adatoms, respectively.

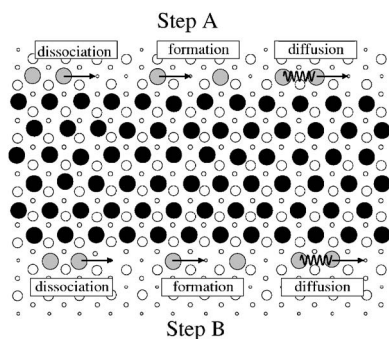| Step	A						B					
Geometry	fcc			hcp			fcc			hcp		
Direction	j	x_0	x_1	j	x_0	x_1	j	x_0	x_1	j	x_0	x_1
▶	507	299	374	508	289	362	510	90	106	510	86	103
◀	1222	1014	1032	1218	999	1016	1228	807	776	1222	799	767

FIG. 8. Atomic motions corresponding to the dissociation, the formation and the concerted diffusion of a Cu dimer along the steps *A* and *B* limiting a stripe in fcc geometry on Cu(111). The atoms are represented as in Fig. 2.

the energy barrier for the dimer formation being around 15% lower than the energy barrier to diffuse freely along a step. Once the dimer is formed the probability for the dimer dissociation is rather low since in any case the associated barrier is larger than 500 meV (see Table V), however a concerted motion of the two atoms is conceivable (see Fig. 8).

We have therefore calculated the energy barrier for the diffusion of such step dimers (Table VI). Interestingly the barrier height for the dimer motion shows a more pronounced anisotropy between step *A* and step *B* than for the single adatom motion. Indeed the ratio of the diffusion barriers along steps *A* and *B* is $\simeq 1.27$ and $\simeq 1.40$ for the single adatom and concerted dimer motions, respectively. In addition the comparison of Tables V and VI shows that the concerted motion of the dimer is easier than the dimer dissociation along step *A*, while along step *B* the dissociation is favored. As a consequence, the dimer diffusion will proceed by concerted motion along step *A*, whereas along step *B* a two step process is preferred, i.e., a dissociation followed by the rebonding of the dimer.

V. DIFFUSION OF ADATOMS ALONG STEPS WITH DEFECTS

When an adatom sticks to the ledges of a preformed close-packed adisland bordered by *A* and *B* steps with defects (kinks or other adatoms) it will in general remain attached to it and, if edge diffusion and corner crossing processes are activated, the adatom will diffuse back and forth between the two types of steps. In the following we will limit ourselves to the study of single and two atoms processes. Even though multiatom mechanisms are conceivable it has been shown by Henkelman and Jónsson[64] that, contrary to

TABLE VI. Diffusion barriers E_{dim} for the dimer diffusion along steps *A* and *B* in fcc and hcp geometries.

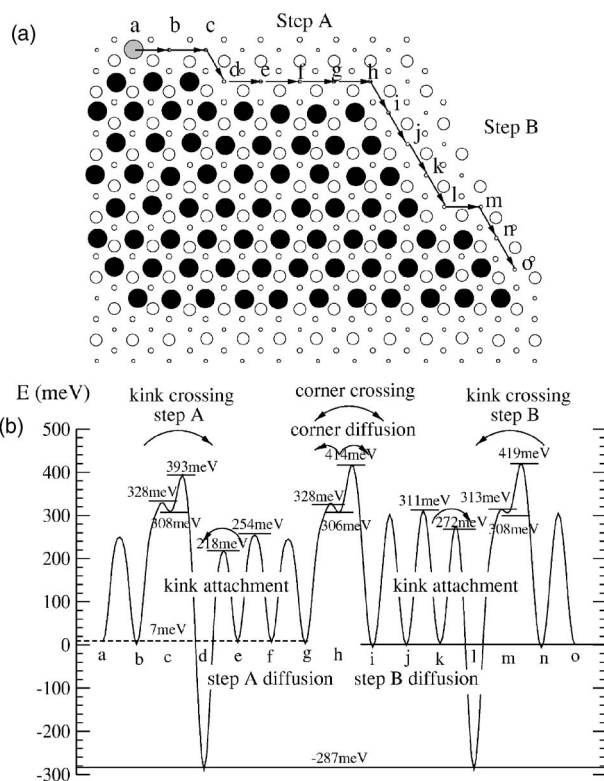| Step	*A*		*B*	
Geometry	fcc	hcp	fcc	hcp
E_{dim} (meV)	463	440	640	625

FIG. 9. (a) A typical diffusion path of an adatom along the borders of an adisland in fcc geometry with *A* and *B* edges on Cu(111), (b) the associated energy profile. The atoms are represented as in Fig. 2.

the growth of Al(100), such processes play a negligible role in the growth of Cu(100). Actually, as we will see below, the exchange processes between two atoms are not energetically favorable, except for very few configurations. We will start by presenting the potential energy profiles for typical diffusion sequences along which the most important processes occur. Then the other diffusion processes will be systematically investigated and the result for their activation barrier will be given and commented on.

A. Typical diffusion sequences

The diffusion path around an adisland in fcc geometry with *A* and (or) *B* borders and the corresponding energy profile is shown in Fig. 9. An adatom starting from step *A* passes around a kink (kink crossing), detaches from this kink, diffuses along step *A* and then passes around a corner between step *A* and step *B* (corner crossing) on which a similar path is followed. Such a sequence is very instructive since the most important processes are encountered (the formation and dissociation of dimers along the steps have been studied in Sec. IV B): (i) diffusion along step *A* ($a \leftrightharpoons b, e \leftrightharpoons f$) and along step *B* ($j \leftrightharpoons k, n \leftrightharpoons o$), (ii) kink crossing on step *A* ($b \rightarrow c \rightarrow d$) and on step *B* ($n \rightarrow m \rightarrow l$), (iii) kink attachment (($e \rightarrow d$ on step *A*, $k \rightarrow l$ on step *B*) or detachment ($d \rightarrow e$ on step *A*, $l \rightarrow k$ on step *B*), (iv) corner crossing ($g \leftrightharpoons h \leftrightharpoons i$).

The energy barriers for the diffusion along step *A* and step *B* have been already studied (Sec. III B). The numerical val-

ues given in Fig. 9(b) are very slightly different (by a few meV) due to the finite size of the adisland edges.

The kink crossing is a two step process since a secondary energy minimum is found at site c on step A and m on step B. The energy barrier to pass around the kink is significantly larger than for the diffusion along straight steps. This is actually the one-dimensional analogue of the Schwoebel effect encountered when diffusing across steps. This means that the adatom is repelled by the descending kink. Furthermore even if the adatom reaches site c on step A, it will most probably come back to site b (barrier, 20 meV) than continue its way to site d (barrier, 85 meV). On the contrary on step B an adatom reaching the site m will most probably continue its way to site l (barrier, 5 meV) rather than turning back to site n (barrier, 111 meV).

The energy barriers for kink detachment are rather high (505 meV for step A, 559 meV for step B) since roughly two nearest neighbor bonds have been broken at the saddle point. Moreover the energy barriers for the kink attachment are significantly lowered (by 30–40 meV) compared with the diffusion barriers of the straight steps since, at the saddle point a bond between the diffusing atom and the kink atom starts to be established. Thus an adatom reaching site e or k has a larger probability to attach to the ascending kink than to be reflected. It is worthwhile to note that this effect cannot be obtained when using approximate expressions for the barriers. Finally it is interesting to compare these energy barriers to those involved in the dissociation and formation of dimers along steps A and B. By comparing with the results of Table V, we see that the kink detachment is easier than the dimer dissociation, while the kink attachment is more difficult than dimer formation. This is clearly due to the change of local atomic environment.

The energy profile for the corner crossing has some similarity with the kink crossing since the energy barrier is significantly larger than for the diffusion along straight steps, i.e., the adatom is repelled by the corner leading to a Schwoebel-type effect. Furthermore a secondary energy minimum is met at site h during the process. However the two minima on both sides of site h (sites g and i) are roughly at the same energy (the energy difference between sites g and i being $\simeq 7$ meV) since both sites have the same first nearest neighbor coordination. Moreover it is interesting to note that an adatom located at site h has a larger probability to escape towards step A (barrier, 22 meV) than towards step B (barrier, 108 meV).

In addition, contrary to the diffusion across the straight steps (see Table IV) the exchange mechanism is never favored compared with the jump process. Indeed, we have already seen (Table I) that the diffusion along steps does not proceed by exchange. Similarly we have verified that the exchange mechanism is also unfavorable for kink and corner crossings. This is illustrated in Fig. 10 for the corner crossing, the usual double jump mechanism ($g \rightarrow h \rightarrow i$) is much preferred to a single [Fig. 10(b)] or double exchange [Fig. 10(c)] mechanism. Surprisingly however the rather unexpected double exchange mechanism is less costly than the single exchange.

Bearing in mind that crystal growth is a kinetic phenomenon leading to out of equilibrium shapes like triangular
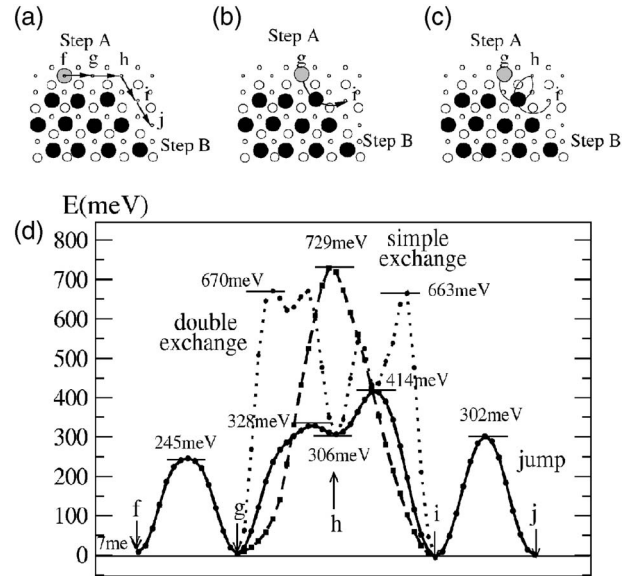

FIG. 10. Possible diffusion mechanisms for passing around the corner between step A and step B on an adisland in fcc geometry on Cu(111), (a) jump process, (b) single exchange, and (c) double exchange mechanisms, (d) the corresponding potential energy profiles, jump (full line), single exchange (dashed line), and double exchange (dotted line). The atoms are represented as in Fig. 2.

adislands, it is also important to study typical diffusion processes occurring in the vicinity of such adisland shapes. For this reason we have also considered the A and B corner crossings around triangular adislands bordered with A or B steps, respectively. The results of our calculation, illustrated in Fig. 11, are quite instructive since it is found that the B corner crossing is much easier than the A one. The asymmetry is $\simeq 100$ meV for the hopping mechanism. This can be understood by looking at the local atomic geometry since at points 2 or 5 the nearest neighbor environment of the diffusing adatom is about the same as on the straight steps and the
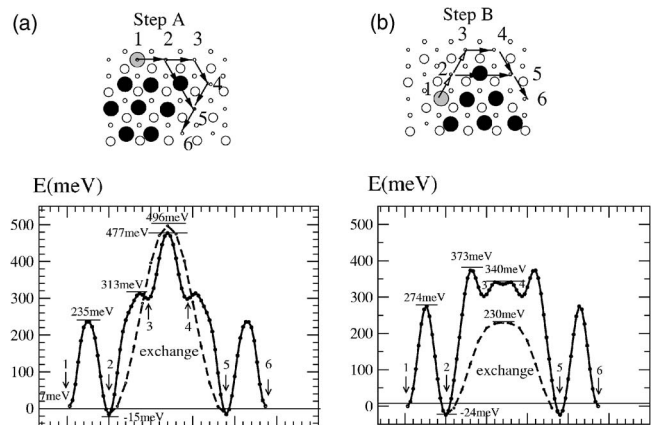

FIG. 11. Upper part, possible diffusion mechanisms (jump and exchange) for passing around A and B corners of a triangular adisland bordered (a) by A steps or (b) B steps, respectively, in fcc geometry on Cu(111). The atoms are represented as in Fig. 2. Lower part, the corresponding potential energy profiles, jump (full line) and exchange (dashed line) mechanisms.
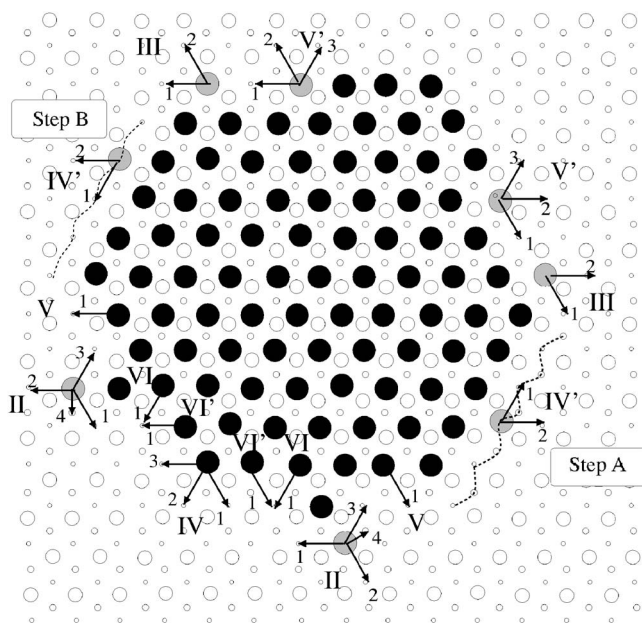
FIG. 12. Diffusion processes of an adatom around an adisland bordered with *A* and *B* steps at fcc sites on Cu(111). The atoms are represented as in Fig. 2.

corresponding energies are very similar as seen in Sec. III B. When going from point 3 to point 4, the nearest neighbor environment of the adatom is similar to that of the saddle point for diffusion along the straight step *B*(*A*) for the *A*(*B*) corner crossing. Consequently the *B* corner crossing is expected to be the easiest one and the difference in the barriers relative to that along straight steps results from a balance between relaxation effects and bond breaking of farther neighbors. As seen in Fig. 11 the asymmetry of diffusion for the corner crossings is even much more pronounced for the exchange mechanism. This can also be explained from the geometrical environment, the exchange mechanism for *A*(*B*) corner crossing is roughly similar to the diffusion of a dimer along *B*(*A*) steps which is highly favored along step *A*. This strong difference in activation energies for *A* and *B* corner crossings could have important consequences on the growth scenario.

B. Other diffusion events

Finally, in view of carrying out a KMC simulation of Cu/Cu(111) growth it is important to have a complete picture of the various diffusion processes. An enumeration of (almost) all diffusion mechanisms (labelled by roman figures) of an adatom in the vicinity of a preformed adisland is presented in Fig. 12. For the sake of completeness we have also considered the possibility for a step edge atom (V, VI, VI′) to escape along the step or a step adatom (IV) to escape on the terrace. We use the following notation hereafter: the initial configuration of the diffusion events represented in Fig. 12 is denoted by an index 0 and the final configuration by an index $i = 1, 2, 3, 4$. For example the simple diffusion of an adatom along a straight step *A* is denoted as $IV'^A_{0 \to 1}$. The arrow is simply reversed for the opposite displacement. Note

that, even though fcc-hcp jumps are the smallest possible diffusion movements, they were not taken into consideration here (except for $II^A_{0 \to 4}$ discussed in the following) since in the vicinity of an adisland all the sites that can be reached by such jumps are unstable, and an adatom situated on such a site would immediately be attracted by the step.

Most of the diffusion processes along steps have already been discussed in detail above and we shall not make any further comment on them. Let us however try to extract some general trends from Table VII.

One can observe that the diffusion energy of an atom in the vicinity of an adisland in hcp geometry is systematically smaller by a few meV than the corresponding energy in the vicinity of an adisland in fcc geometry similarly to the diffusion along straight steps.

Obviously, the energy necessary for an atom to leave an adisland towards the terrace and lose all its first nearest neighbors from the adisland, is much higher than the diffusion energy along steps. Indeed the energy cost of such processes is around 950 meV for a corner ($IV_{0 \to 2}$) or a kink atom ($V'_{0 \to 2}$), around 650 meV for a step adatom to escape on the terrace ($IV'_{0 \to 2}$) and decreases to 400 meV for the motion $II^B_{0 \to 2}$. These energy barriers obviously decrease with the number of bonds lost in the diffusion process which are equal to 3, 2, and 1, respectively. However this correlation is very approximate since, for a given number of broken bonds, the values of the activation barriers vary over a rather large interval, for instance, when a single bond is broken the activation barrier lies between 323 and 560 meV. Indeed, similarly to the case of straight steps, the potential energy surface of an adatom is strongly affected by the vicinity of the adisland. As a consequence the diffusion path cannot be guessed from symmetry arguments and, at the saddle point, many different interatomic distances with the neighbors are involved so that it is difficult to derive an effective pair interaction model as done in our previous work.[22] Let us also stress that the terrace site that can be reached from an adisland site may be unstable or quasiunstable, see, for example, the diffusion processes $IV_{0 \leftarrow 2}$ and $V'_{0 \leftarrow 2}$ for both steps.

Finally let us mention that the $II^A_{0 \to 4}$ process is also affected by the presence of the adisland. Indeed the energy profile would be very different if the diffusing atom and its nearest neighbor were isolated on the terrace. The dimer motion was studied in detail in our previous work[22] and the energy barrier corresponding to a motion of type $II_{0 \to 4}$ from an fcc-fcc to an fcc-hcp configuration (also called ff-fh in Refs. 22 and 30) was found equal to 16 meV (the initial and final sites being almost energetically degenerate), whereas in the presence of an adisland this motion becomes highly asymmetrical, and the true dimer (fcc-fcc) is stabilized by the vicinity of the adisland. This phenomenon is similar with the experimental finding of Repp *et al.*[30] who observed the stabilization of a dimer by the proximity of a monomer. In the case of $II^B_{0 \to 4}$ the influence of the step atoms is so strong that the final site becomes unstable.

VI. CONCLUSION

In conclusion, we have carried out a systematic study of the diffusion processes that can occur for a Cu adatom in the

TABLE VII. Calculated diffusion barriers for a Cu adatom jumping from an initial site 0 to a final site (1, 2, 3, or 4) and vice versa. ΔZ is the number of nearest neighbor bonds broken in the diffusion process, i.e., between the initial and final site. The various diffusion events are shown in Fig. 12.

Diffusion event		ΔZ	A		B	
			fcc	hcp	fcc	hcp
II	$0 \to 1$	0	38	33	189	180
	$0 \leftarrow 1$		38	33	189	180
	$0 \to 2$	1	400	396	411	405
	$0 \leftarrow 2$		30	28	32	29
	$0 \to 3$		60	54	3	3
	$0 \leftarrow 3$	2	668	660	600	602
	$0 \to 4$		39	33		
	$0 \leftarrow 4$		6	10		
III	$0 \to 1$	1	327	323	424	415
	$0 \leftarrow 1$		21	17	113	104
	$0 \to 2$	2	667	664	689	686
	$0 \leftarrow 2$		3	1	17	16
IV	$0 \to 1$	2	609	606	609	606
	$0 \leftarrow 1$		10	9	10	9
	$0 \to 2$	3	952	948	952	948
	$0 \leftarrow 2$		0	0	0	0
	$0 \to 3$	2	695	685	695	685
	$0 \leftarrow 3$		94	87	94	87
IV'	$0 \to 1$	0	247	235	312	302
	$0 \leftarrow 1$		247	235	312	302
	$0 \to 2$	2	660	661	683	677
	$0 \leftarrow 2$		0.6	0.7	19	15
V	$0 \to 1$	3	913	903	866	862
	$0 \leftarrow 1$		45	40	0	0
V'	$0 \to 1$	1	506	494	560	551
	$0 \leftarrow 1$		211	200	270	262
	$0 \to 2$	3	950	947	947	945
	$0 \leftarrow 2$		0	0	0	0
	$0 \to 3$	2	681	674	600	599
	$0 \leftarrow 3$		86	80	8	7
VI	$0 \to 1$	3	842	837	824	816
	$0 \leftarrow 1$		45	43	19	16
VI'	$0 \to 1$	2	726	713	647	633
	$0 \leftarrow 1$		196	183	114	103

presence of a close-packed adisland on Cu(111). In view of the small value of the stacking fault energy in Cu, two geometries have been considered in which the atoms of the adisland occupy fcc or hcp sites. The diffusion rates along step A and step B without defects have been first investigated using TST-HA and MD simulations in the classical limit.

They obey Arrhenius laws with activation barriers significantly larger along step B than along step A. Whereas the (static) potential energy barriers account for the slope of the MD Arrhenius plots within statistical errors, the attempt frequencies are markedly different due to the anharmonic and recrossing effects included in MD simulations. Indeed, in contrast with the Vineyard attempt frequencies which have similar values for all geometries, the prefactors derived from MD simulations obey the Meyer-Neldel compensation rule, i.e., the increase of the activation barrier for B steps compared with A steps is somewhat compensated by an increase of the prefactor. Furthermore, the law proposed by Boisvert et al.[36] to relate the activation barrier to the prefactor accounts quite well for our results. Consequently we have then limited ourselves to the determination of static potential barriers for a large number of diffusion events that can occur in the presence of an adisland. A number of additional differences have been put forward between the diffusion along A and B borders which may have an influence on the adisland growth shapes. In agreement with previous EAM calculations[47] we find that the exchange mechanism for descending a step is largely favored, especially on step B for which the Schwoebel extra barrier is only $\simeq 50-60$ meV. Moreover it is shown that the corner crossing diffusion process by jump or exchange for triangular adislands with A borders have a similar and high ($\simeq 480$ meV) activation barriers while for triangular adislands with B borders the exchange mechanism is largely favored and has a rather low barrier (230 meV). From this set of results the diffusion rates of the most important atomic displacements can be predicted and used as input in KMC simulations which are currently in progress.

APPENDIX

Let us consider the ($3N+3$-dimensional) configuration space of a system with $N+1$ identical atoms of mass m and assume that the potential energy of this system has two minima at points A and B separated by a saddle point P. We suppose that the dividing surface Σ_P (containing P) between the regions A and B as well as the diffusion path (i.e., the steepest descent line going from A to B through P) have been determined (see Fig. 13). The coordinate system is chosen so that one coordinate, s, runs along the diffusion path. The equation of Σ_P is then $s = s_P$. In the transition state theory the diffusion rate from A to B is given by[49]

$$\Gamma_{\text{TST}}^{A \to B}(T) = \frac{\langle v_s \theta(v_s) \delta(s - s_P) \rangle}{\langle \theta(s_P - s) \rangle}, \qquad (A1)$$

where v_s is the velocity along s, $\langle \cdots \rangle$ denotes a canonical average and θ is the Heaviside function.

The basic assumption leading to Eq. (A1) is that each crossing of Σ_P corresponds to a diffusion event. This is not true since recrossing may occur before thermalization in re-
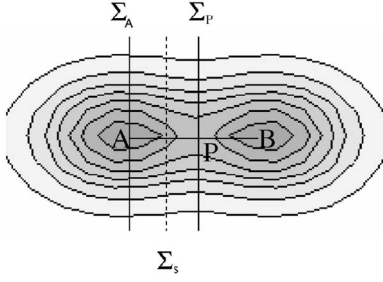
FIG. 13. Schematic potential energy surfaces in the vicinity of two potential wells A and B separated by a saddle point P. The surfaces Σ_s are given by $s=$cst where s is the coordinate along the diffusion path.

gion B. To correct for this effect a transmission coefficient $\kappa(T)$ is introduced so that the total diffusion rate is

$$\Gamma(T) = n_c \kappa(T) \Gamma_{\text{TST}}^{A \to B}(T) \qquad (A2)$$

when there are n_c diffusion channels.

Diffusion rate in the TST-HA

When integrating over $p_s = m v_s$ in the canonical average of the numerator of Eq. (A1), $\Gamma_{\text{TST}}^{A \to B}(T)$ can be rewritten

$$\Gamma_{\text{TST}}^{A \to B}(T) = \frac{k_B T}{h} \frac{Z_{\Sigma_P}}{Z_A}, \qquad (A3)$$

where Z_{Σ_P} is a *constrained* partition function, i.e., in which the representative points of the system in the $3N+3$-dimensional configuration space are compelled to stay on Σ_P and Z_A is the partition function when the representative points are located in the region around A. Thus the dimensionality of the configuration space is $3N+2$ for Z_{Σ_P} and $3N+3$ for Z_A.

If the static barrier ΔE is much larger than $k_B T$, the HA can be used and $\Gamma_{\text{TST}}^{A \to B}(T)$ becomes

$$\Gamma_{\text{TST}}^{A \to B}(T) = \frac{k_B T}{h} \exp[-(\Delta E + \Delta F_{\text{vib}})/k_B T], \qquad (A4)$$

where $\Delta F_{\text{vib}} = \Delta U_{\text{vib}} - T \Delta S_{\text{vib}}$ is the contribution of vibrations to the free energy, with

$$\Delta U_{\text{vib}} = \int_0^{\nu_{\text{max}}} \frac{h\nu}{2} \coth\left(\frac{h\nu}{2k_B T}\right) \Delta n(\nu) d\nu,$$

$$\Delta S_{\text{vib}} = k_B \int_0^{\nu_{\text{max}}} \left\{ \frac{h\nu}{2k_B T} \coth\left(\frac{h\nu}{2k_B T}\right) \right.$$
$$\left. - \ln\left[2 \sinh\left(\frac{h\nu}{2k_B T}\right)\right] \right\} \Delta n(\nu) d\nu, \qquad (A5)$$

and

$$\int_0^{\nu_{\text{max}}} \Delta n(\nu) d\nu = -1. \qquad (A6)$$

Indeed, in the HA the constraint on Z_{Σ_P} can be expressed as $q_P = 0$ where q_P is the normal coordinate corresponding to

the unstable mode at point P. As a consequence this mode must be excluded from the summation over ν. Consequently, in this approximation and in the classical limit

$$\Delta U_{\text{vib}} = -k_B T, \qquad (A7)$$

$$\Delta S_{\text{vib}} = -k_B \left(1 - \ln \frac{h\nu_0}{k_B T}\right), \qquad (A8)$$

where ν_0 is the Vineyard attempt frequency [Eq. (11)]. These quantities have been calculated explicitly for self-diffusion on the (100) surface of Cu and Ag.[32,33] Finally note that the correction factor $\kappa(T)$ is generally omitted in the HA.

Diffusion rate from the TI method

In this approach, the integration over all momenta in both canonical averages of Eq. (A1) is carried out in the classical limit. This leads to

$$\Gamma_{\text{TST}}^{A \to B}(T) = \left(\frac{k_B T}{2\pi m}\right)^{1/2} \frac{\int_{\Sigma_P} \exp[-E(\cdots r_{ij} \cdots)/k_B T] d\Sigma_P}{\int_{V_A} \exp[-E(\cdots r_{ij} \cdots)/k_B T] dV_A}. \qquad (A9)$$

The integration domain extends over the hypersurface Σ_P in the numerator and the hypervolume V_A limited by Σ_P and containing A in the denominator. Let Σ_s be the surface $s=cst$, i.e., it is normal at s to the steepest descent line containing A and P and set

$$C \exp[-W(s)/k_B T] = \int_{\Sigma_s} \exp[-E(\cdots r_{ij} \cdots)/k_B T] d\Sigma_s, \qquad (A10)$$

where C is a constant. If we multiply the numerator and denominator of Eq. (A9) by $\exp[-W(s_A)/k_B T]$, this equation can be rewritten as

$$\Gamma_{\text{TST}}^{A \to B}(T) = \left(\frac{k_B T}{2\pi m}\right)^{1/2} \left(\int_{-\infty}^{s_P} \exp\{-[W(s) - W(s_A)]/k_B T\} ds\right)^{-1}$$
$$\times \exp\{-[W(s_P) - W(s_A)]/k_B T\} \qquad (A11)$$

$$= \nu(T) \exp(-\Delta W/k_B T). \qquad (A12)$$

The constant C can be fixed by setting $W(s_A)=0$. Thus

$$W(s) = -k_B T \ln \frac{\int_{\Sigma_s} \exp[-E(\cdots r_{ij} \cdots)/k_B T] d\Sigma_s}{\int_{\Sigma_A} \exp[-E(\cdots r_{ij} \cdots)/k_B T] d\Sigma_A}. \qquad (A13)$$

The function $W(s)$ is known as the "potential of mean force"[65] in the literature. Indeed it is straightforward to show that

$$\frac{dW}{ds} = \left\langle \frac{\partial E}{\partial s} \right\rangle. \tag{A14}$$

Finally $\Delta W = W(s_P) - W(s_A)$ is an activation free energy which satisfies

$$\exp(-\Delta W/k_B T) = \frac{Z_{\Sigma_P}}{Z_{\Sigma_A}} \tag{A15}$$

in which both Z_{Σ_P} and Z_{Σ_A} are now *constrained* partition functions having thus the same dimensionality $(3N+2)$ of the configuration space. Note that this point of view is closely related to the formulation of Wert and Zener.[52,66] We must

emphasize that if we set $\Delta W = \Delta E + \Delta U^{\mathrm{TI}} - T\Delta S^{\mathrm{TI}}$, the quantities ΔU^{TI} and ΔS^{TI} are different from ΔU_{vib} and ΔS_{vib} [Eq. (A8)] even in the HA. Indeed the number of modes, being the same in the two partition functions, $\Delta U_{\mathrm{HA}}^{\mathrm{TI}}$ vanishes and $\Delta S_{\mathrm{HA}}^{\mathrm{TI}}$ is independent of temperature.

This method has been used by Boisvert *et al.*[34] for the diffusion of Cu on Cu(100) without resorting to the HA. They used MD simulations to calculate ΔW, $\nu(T)$, and $\kappa(T)$ and showed that their result for $\Gamma(T)$ [Eq. (A2)] can be fitted nicely by an Arrhenius law. Indeed they found that (i) if ΔW is written as $\Delta E^{\mathrm{TI}} - T\Delta S^{\mathrm{TI}}$, then ΔE^{TI} and ΔS^{TI} are both *effectively* temperature independent, (ii) $\kappa(T)$ and $\nu(T)$ are only slightly dependent on temperature.

[1] Z. Zhang and M. G. Lagally, Science **276**, 377 (1997), and references therein.

[2] M. Giesen, Prog. Surf. Sci. **68**, 1 (2001), and references therein.

[3] O. V. Lysenko, V. S. Stepanyuk, W. Hergert, and J. Kirschner, Phys. Rev. Lett. **89**, 126102 (2002).

[4] S. Liu, Z. Zhang, G. Comsa, and H. Metiu, Phys. Rev. Lett. **71**, 2967 (1993).

[5] M. Villarba and H. Jónsson, Surf. Sci. **317**, 15 (1994).

[6] J. Jacobsen, K. W. Jacobsen, and J. K. Nørskov, Surf. Sci. **359**, 37 (1996).

[7] T. Michely, M. Hohage, M. Bott, and G. Comsa, Phys. Rev. Lett. **70**, 3943 (1993).

[8] A. Gölzhäuser and G. Ehrlich, Phys. Rev. Lett. **77**, 1334 (1996).

[9] W. Wulfhekel, N. N. Lipkin, J. Kliewer, G. Rosenfeld, L. C. Jorritsma, B. Poelsema, and G. Comsa, Surf. Sci. **348**, 227 (1996).

[10] D. C. Schlößer, K. Morgenstern, L. K. Verheij, G. Rosenfeld, F. Besenbacher, and G. Comsa, Surf. Sci. **465**, 19 (2000).

[11] M. Giesen and H. Ibach, Surf. Sci. **529**, 135 (2003).

[12] B. D. Yu and M. Scheffler, Phys. Rev. Lett. **77**, 1095 (1996).

[13] K. A. Fichthorn and M. Scheffler, Phys. Rev. Lett. **84**, 5371 (2000).

[14] S. Papadia, B. Piveteau, D. Spanjaard, and M. C. Desjonquères, Phys. Rev. B **54**, 14720 (1996).

[15] S. C. Wang and G. Ehrlich, Surf. Sci. **239**, 301 (1990).

[16] F. Máca, M. Kotrla, and O. S. Trushin, Surf. Sci. **454–456**, 579 (2000).

[17] R. Stumpf and M. Scheffler, Phys. Rev. B **53**, 4958 (1996).

[18] P. Ruggerone, A. Kley, and M. Scheffler, Prog. Surf. Sci. **54**, 331 (1997).

[19] S. Ovesson, A. Bogicevic, and B. I. Lundqvist, Phys. Rev. Lett. **83**, 2608 (1999).

[20] Y. Li and A. E. DePristo, Surf. Sci. **351**, 189 (1996).

[21] Y. Mishin, M. J. Mehl, D. A. Papaconstantopoulos, A. F. Voter, and J. D. Kress, Phys. Rev. B **63**, 224106 (2001).

[22] M. C. Marinica, C. Barreteau, M. C. Desjonquères, and D. Spanjaard, Phys. Rev. B **70**, 075415 (2004).

[23] F. Raouafi, C. Barreteau, M. C. Desjonquères, and D. Spanjaard, Surf. Sci. **505**, 183 (2002).

[24] A. Bortz, M. Kalos, and J. Lebowitz, J. Comput. Phys. **17**, 10 (1975).

[25] P. Jensen, Rev. Mod. Phys. **71**, 1695 (1999).

[26] J. M. Pomeroy, J. Jacobsen, C. C. Hill, B. H. Cooper, and J. P. Sethna, Phys. Rev. B **66**, 235412 (2002).

[27] K. Stolt, W. R. Graham, and G. Ehrlich, J. Chem. Phys. **65**, 3206 (1976).

[28] G. Antczak and G. Ehrlich, Phys. Rev. Lett. **92**, 166105 (2004).

[29] T. R. Linderoth, S. Horch, E. Lægsgaard, I. Stensgaard, and F. Besenbacher, Phys. Rev. Lett. **78**, 4978 (1997).

[30] J. Repp, G. Meyer, K. H. Rieder, and P. Hyldgaard, Phys. Rev. Lett. **91**, 206102 (2003).

[31] U. Kürpick, A. Kara, and T. S. Rahman, Phys. Rev. Lett. **78**, 1086 (1997).

[32] U. Kürpick and T. S. Rahman, Surf. Sci. **383**, 137 (1997).

[33] U. Kürpick and T. S. Rahman, Phys. Rev. B **57**, 2482 (1998).

[34] G. Boisvert, N. Mousseau, and L. J. Lewis, Phys. Rev. B **58**, 12667 (1998).

[35] R. Ferrando and G. Tréglia, Phys. Rev. B **50**, 12104 (1994).

[36] G. Boisvert, L. J. Lewis, and A. Yelon, Phys. Rev. Lett. **75**, 469 (1995).

[37] G. Boisvert and L. J. Lewis, Phys. Rev. B **54**, 2880 (1996).

[38] G. Boisvert and L. J. Lewis, Phys. Rev. B **56**, 7643 (1997).

[39] F. Montalenti and R. Ferrando, Phys. Rev. B **59**, 5881 (1999).

[40] M. I. Larsson, Phys. Rev. B **64**, 115428 (2001).

[41] F. Grosse, W. Barvosa-Carter, J. J. Zinck, and M. F. Gyure, Phys. Rev. B **66**, 075321 (2002).

[42] V. N. Antonov, J. S. Palmer, P. S. Waggoner, A. S. Bhatti, and J. H. Weaver, Phys. Rev. B **70**, 045406 (2004).

[43] W. Meyer and H. Neldel, Z. Tech. Phys. (Leipzig) **12**, 588 (1937).

[44] C. Ratsch and M. Scheffler, Phys. Rev. B **58**, 13163 (1998).

[45] P. Stoltze, J. Phys.: Condens. Matter **6**, 9495 (1994).

[46] M. Karimi, T. Tomkowski, G. Vidali, and O. Biham, Phys. Rev. B **52**, 5364 (1995).

[47] O. S. Trushin, K. Kokko, P. T. Salo, W. Hergert, and M. Kotrla, Phys. Rev. B **56**, 12135 (1997).

[48] G. A. Evangelakis, D. G. Papageorgiou, G. C. Kallinteris, C. E. Lekka, and N. I. Papanicolaou, Vacuum **50**, 165 (1998).

[49] G. Wahnström, in *Interaction of Atoms and Molecules with Solid Surfaces*, edited by V. Bortolani, N. H. March, and M. P. Tosi (Plenum, New York, London, 1990), p. 529.

[50] A. Ulitsky and R. Elber, J. Chem. Phys. **92**, 1510 (1990).

[51] D. Pines, *Elementary Excitations in Solids* (Benjamin, New York, Amsterdam, 1964).

[52] G. H. Vineyard, J. Phys. Chem. Solids **3**, 121 (1957).

[53] C. Kittel, *Introduction to Solid State Physics* (Wiley, New York, 1971).

[54] C. Z. Wang, C. T. Chan, and K. M. Ho, Phys. Rev. B **42**, 11276 (1990).

[55] F. Raouafi, C. Barreteau, D. Spanjaard, and M. C. Desjonquères, Phys. Rev. B **66**, 045410 (2002).

[56] M. C. Desjonquères and D. Spanjaard, *Concepts in Surface Physics* (Springer-Verlag, Berlin, New York, 1996), Sec. 5.4.4.

[57] V. Rosato, M. Guillopé, and B. Legrand, Philos. Mag. A **59**, 301 (1989).

[58] D. Emin, Phys. Rev. Lett. **32**, 303 (1974).

[59] A. Yelon, B. Movaghar, and H. M. Branz, Phys. Rev. B **46**, 12244 (1992).

[60] Note that for Cu on Cu(100) the motion is two dimensional and consequently the diffusion coefficient $D(T)$ and the diffusion frequency $\Gamma(T)$ are related by $D(T)=a^2\Gamma(T)/4$.

[61] M. Giesen and H. Ibach, Surf. Sci. **431**, 109 (1999).

[62] X. F. Gong, L. Wang, X. J. Ning, and J. Zhuang, Surf. Sci. **553**, 181 (2004).

[63] O. V. Lysenko, V. S. Stepanyuk, W. Hergert, and J. Kirschner, Phys. Rev. B **68**, 033409 (2003).

[64] G. Henkelman and H. Jónsson, Phys. Rev. Lett. **90**, 116101 (2003).

[65] B. Roux and M. Karplus, Biophys. J. **59**, 961 (1991); J. Phys. Chem. **95**, 4856 (1991).

[66] C. Wert and C. Zener, Phys. Rev. **76**, 1169 (1949).